AD-A043 909 LEHIGH UNIV BETHLEHEM PA INST OF FRACTURE AND SOLID --ETC F/G 20/1.
MECHANICS OF DUCTILE FRACTURE.(U)
JUN 77 G C SIH
UNCLASSIFIED IFSM-77-78 N00014-76-C-0094
NL

END
DATE FILMED
9 -77
DDC

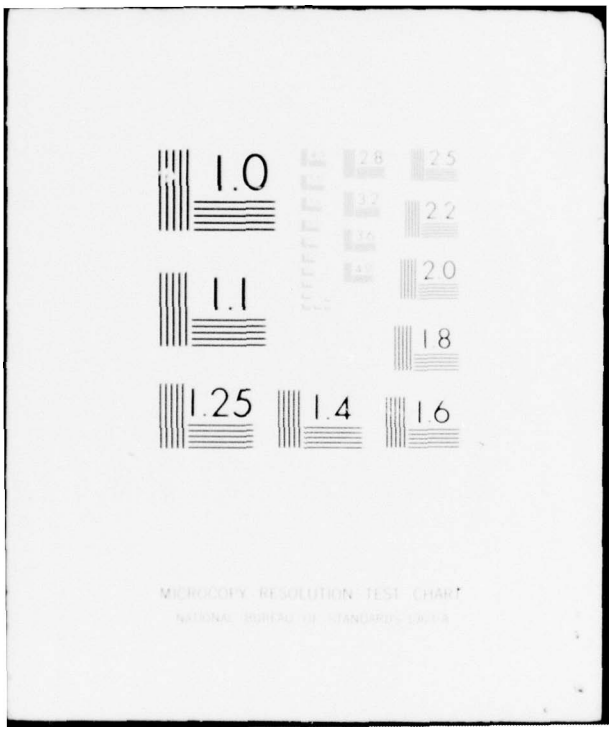
1.0
1.1
1.25
1.4
1.6
2.0
2.2
2.5
2.8
3.2
3.6
4.0
MICROCOPY RESOLUTION TEST CHART
NATIONAL BUREAU OF STANDARDS 1963-A

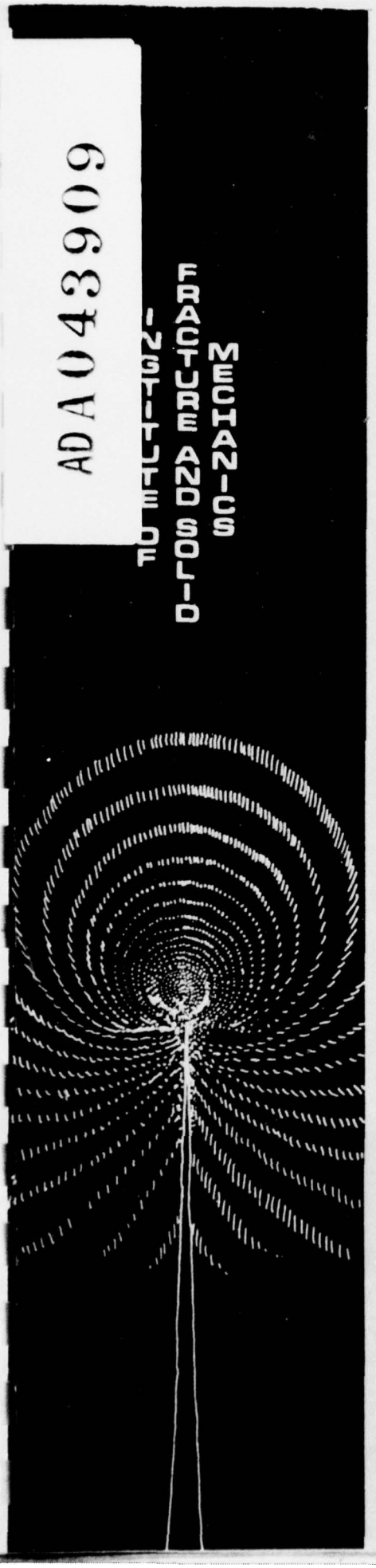

IFSM-77-78

LEHIGH UNIVERSITY

MECHANICS OF DUCTILE FRACTURE

BY

G. C. SIH

TECHNICAL REPORT

JUNE 1977

DEPARTMENT OF THE NAVY
OFFICE OF NAVAL RESEARCH
ARLINGTON, VIRGINIA 22217

(6) MECHANICS OF DUCTILE FRACTURE.

by

(10) G. C./Sih

LEHIGH UNIVERSITY

Institute of Fracture and Solid Mechanics

Bethlehem, Pennsylvania 18015

(11) June 1977 (12) 22p.

(14) IFSM-77-78

(9) Technical Report,

Prepared under Contract N00014-76-C-0094
(15)
for

Department of the Navy

Office of Naval Research

Arlington, Virginia 22217

LB

MECHANICS OF DUCTILE FRACTURE

G. C. Sih
Lehigh University, Bethlehem, Pennsylvania 18015

INTRODUCTION

There are a number of ways in which a metal can deform and/or break into separate pieces. Even in a simple tensile test, wide variations can be found in the mode of failure depending on the material and operational conditions. Single crystals of soft metals such as lead and gold tend to neck and thin out to a fine point before separation takes place, Figure 1(a). This process of surface creation is more appropriately described as deformation rather than fracture and is relatively simple to analyze which will not be discussed further. At the other extreme for materials such as glass and hardened steels, very little deformation is observed before breaking, Figure 1(b). The more common types of fracture are those occurring in polycrystalline materials which show some necking or deformation and then break leaving fracture surfaces* with a characteristic shape such as a cup-and-cone shown in Figure 1(c).

The situation in Figure 1(c) is most complex and cannot be adequately treated by the classical fracture mechanics theory [1] originally proposed to explain brittle fracture. Deformation of moderately ductile metals is normally accomplished by the formation of tiny cavities or voids that eventually coalesce to form a macrocrack in a plane normal to the applied load, although this may be a zig-zag shape on a microscopic scale. As this crack moves towards the free surface, triaxial stresses are set up in the material and the specimen undergoes both shape change (distortion) and volume change (dilatation). This process continues until an instability point is reached at which time the crack runs out of the specimen at an angle to the original crack plane, Figure 1(c). This change of direction may either form the cone on the upper half and cup on the lower half of the specimen or vice versa. The choice depends on a small nonalignment of the crack with the mid-plane of loading as discussed in [2,3].

*The problem of whether the fracture is transgranular or intergranular will not be addressed here since the analysis to follow will not include the microstructure of the material.

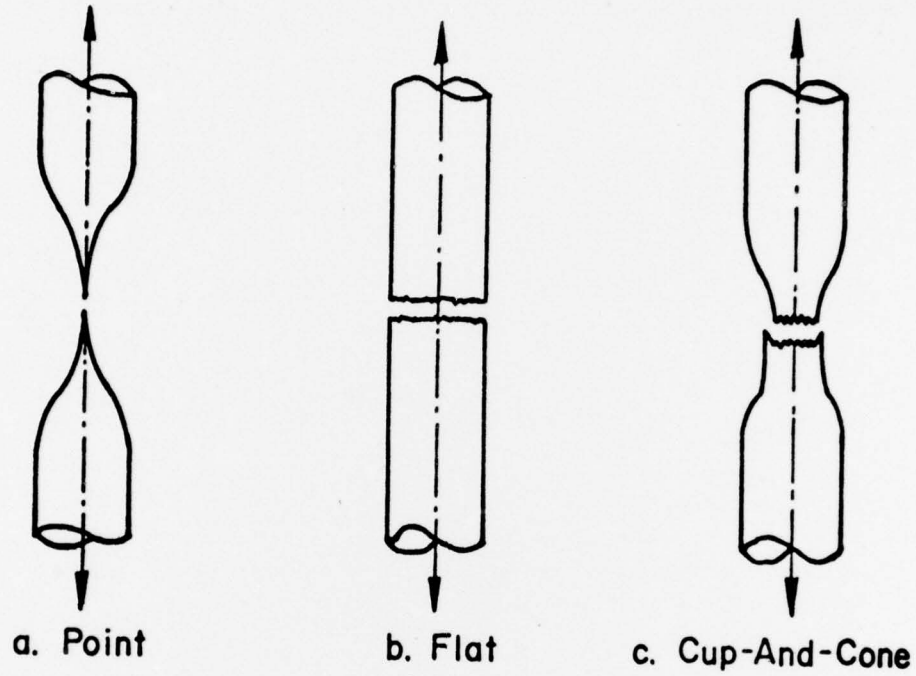

Fig. (1) - Types of fracture

A similar phenomenon is observed in the fracture of moderately thick plate specimens with a through crack such that the combinations of material properties and plate geometry would not satisfy the ASTM requirements [4] for plane strain where the smallest geometric length parameter must be greater or equal to $2.5(K_{1c}/\sigma_{ys})^2$. Here, K_{1c} is the valid critical Mode I stress intensity factor and σ_{ys} the yield strength of the material. Figure 2 shows that the critical stress intensity factor K_c^* becomes K_{1c} or geometry independent only when the plate is sufficiently thick. The fracture surface appearance as shown in Figure 3(a) is almost all flat, i.e., the through crack grows in its initial plane normal to the applied load. As the plate thickness is decreased, the crack will initially tunnel and then deviate from its own plane near the plate surfaces forming "shear lips". The crack growth is stable at first advancing from its initial configuration in a planar fashion marked by the dotted area in Figure

---

*K_c should not be referred to as the plane stress fracture toughness value because the mode of fracture for this specimen is in no way related to the plane stress plasticity crack solution.

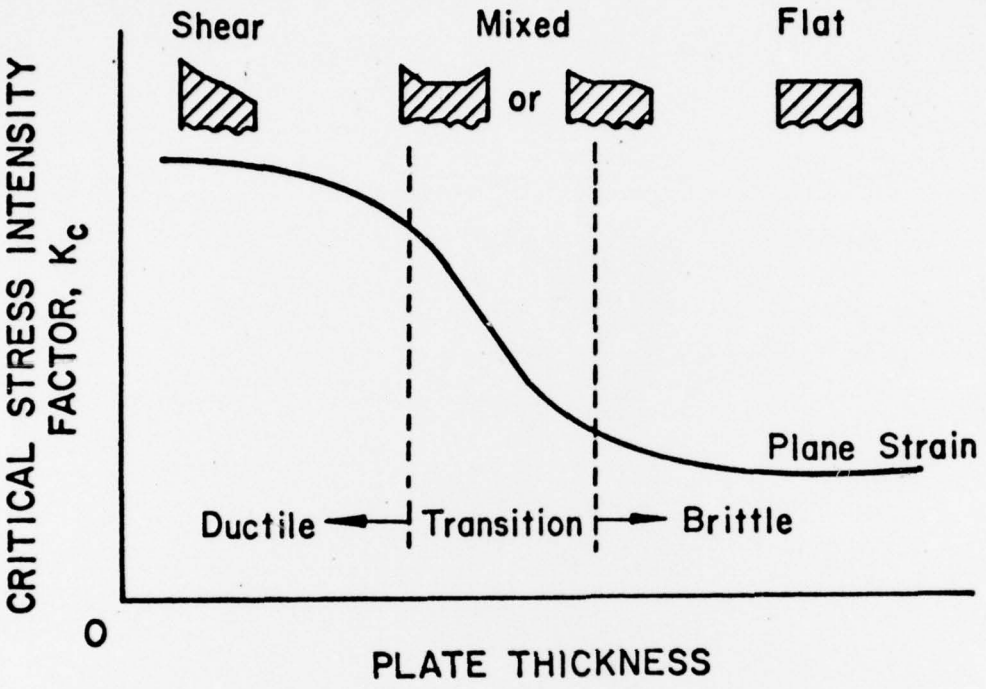

Fig. (2) - Variation of K_c with plate thickness

3(b) with a curved front. Upon reaching the point of instability, the curved crack breaks through the plate. This can be traced on the loading history curve. Again local conditions will determine whether the shear lip will form on one crack surface or the other. Further reduction in plate thickness leads to the decrease of flat surface, Figure 1(c), and a slanted fracture pattern is finally observed.

In order to predict the aforementioned ductile fracture phenomenon, it is necessary to have a fracture criterion that is amenable to analyzing mixed mode crack propagation. The regions of distortion must be distinguished from those undergoing large dilatation such that prediction on crack trajectory can be made. On physical grounds, distortion is associated with yielding of the material while dilatation is associated with crack propagation. Figures 4(a) and 4(b) show that under symmetric loading distortion or yielding is off to the sides of the crack and dilatation leading to fracture is directly ahead. A description of the ductile fracture process involves the interplay between yielding and crack growth which is fundamental to the understanding of transition from slow to rapid crack propagation. That problem is difficult because it not only requires a three-dimensional elastic-plastic analysis of a finite width and/or thickness specimen containing a growing crack but a realistic fracture criterion.

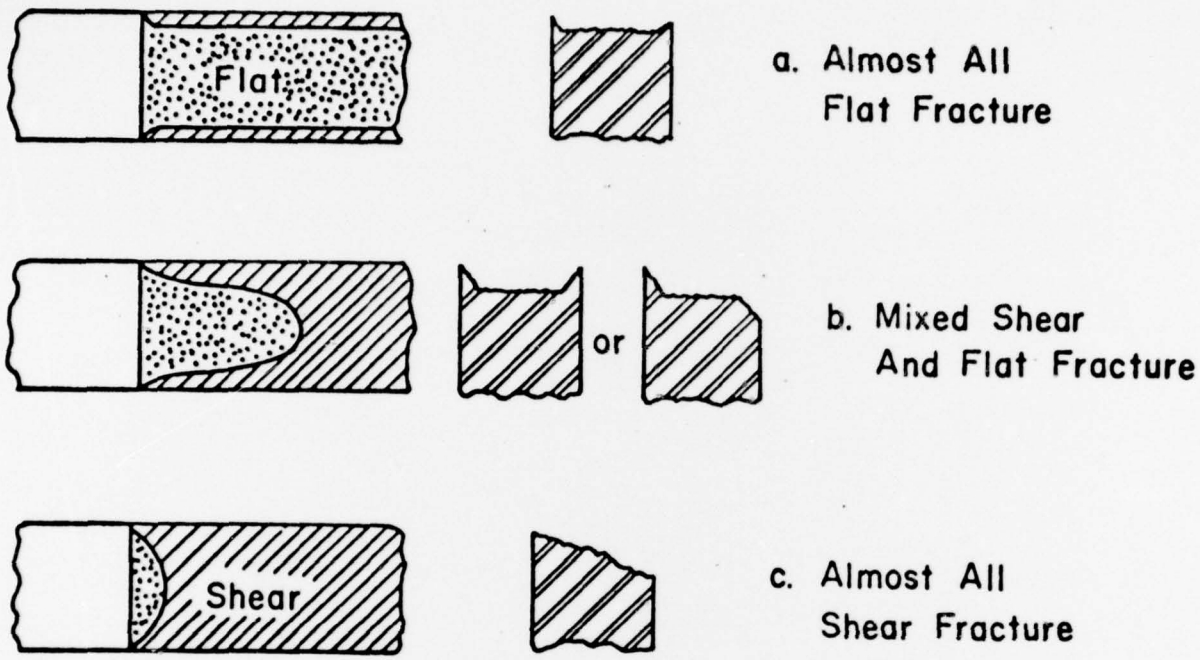

Fig. (3) - Appearance of fracture surfaces

ELASTIC-PLASTIC STRESS ANALYSIS

In order to gain insight into the shear lip formation process, a two-dimensional elastic-plastic stress analysis [5] is carried out to investigate the phenomenon of crack turning during the last ligament growth when it approaches the specimen surface.

The numerical calculation is based on a two-dimensional finite element program employing the twelve node isoparametric element. A special crack tip element is employed where use is made of the singularity solution [6] for the stresses and strains

$$\sigma_{ij} = \frac{K}{r^{1/(1+n)}} \sigma_{ys} f_{ij}(\theta)$$

$$\varepsilon_{ij} = \frac{K^n}{r^{1/(1+n)}} \frac{\alpha\sigma_{ys}}{E} g_{ij}(\theta) \qquad (1)$$

while the displacements

$$u_i = K^n r^{1/(1+n)} \frac{\alpha\sigma_{ys}}{E} h_i(\theta) \tag{2}$$

are finite as $r \to 0$, the crack tip. When the power hardening exponent n=1, the functions $f_{ij}(\theta)$, $g_{ij}(\theta)$ and $h_i(\theta)$ reduce to those for the elastic case with θ being the polar angle measured from the line of expected crack extension under symmetric loading. For the elastic-plastic problem, the coefficient* K does not have the same meaning as stress (or strain) intensity factor used in the elastic case. In Eqs. (1) and (2), E is the Young's modulus and α is a material parameter employed in the J_2 deformation theory of plasticity:

$$e_{ij} = \frac{1+\nu}{E} s_{ij} + \frac{3}{2}\frac{\alpha}{E}\left[\left(\frac{\sigma_{eff}}{\sigma_{ys}}\right)^{n-1} - \frac{\sigma_{ys}}{\sigma_{eff}}\right] s_{ij} \tag{3}$$

where σ_{eff} is the effective stress. The strain and stress deviators are given by

$$e_{ij} = \varepsilon_{ij} - \frac{1}{3}\varepsilon_{pp}\delta_{ij}, \quad s_{ij} = \sigma_{ij} - \frac{1}{3}\sigma_{pp}\delta_{ij} \tag{4}$$

with $\varepsilon_{pp} = [(1-2\nu)/E]\sigma_{pp}$ and ν is the Poisson's ratio. Hence, the particular elastic-plastic material behavior is completely determined by specifying E, α and n.

CENTER CRACK SPECIMEN

For the purpose of numerical calcuation, a center crack specimen with dimensions of 4 in by 4 in is considered. The specimen contains a crack of length 2a while 2b designates the specimen width. The far field stress is oriented uniaxially normal to the crack with a magnitude σ_o. Material parameters are selected to take the following values:

$E = 1$ psi, $\sigma_{ys} = 1$ psi

$\alpha = 0.5$, $\nu = 0.3$ and $n = 5.0$

*The choice of using K, K^n or some combination of K and K^n as a fracture criterion is not clear. It should be cautioned that the form of the singular solution in Eqs. (1) and (2) was made possible only by assuming that the material in a small circular or core region surrounding the crack tip yields uniformly. This is obviously not the case. The consequence of such an assumption as to how it would affect the results in a qualitative and quantitative manner has not been studied and is still not known. Hopefully, the finite element solution based on Eqs. (1) and (2) would not be affected seriously at a distance sufficiently far from the core region.

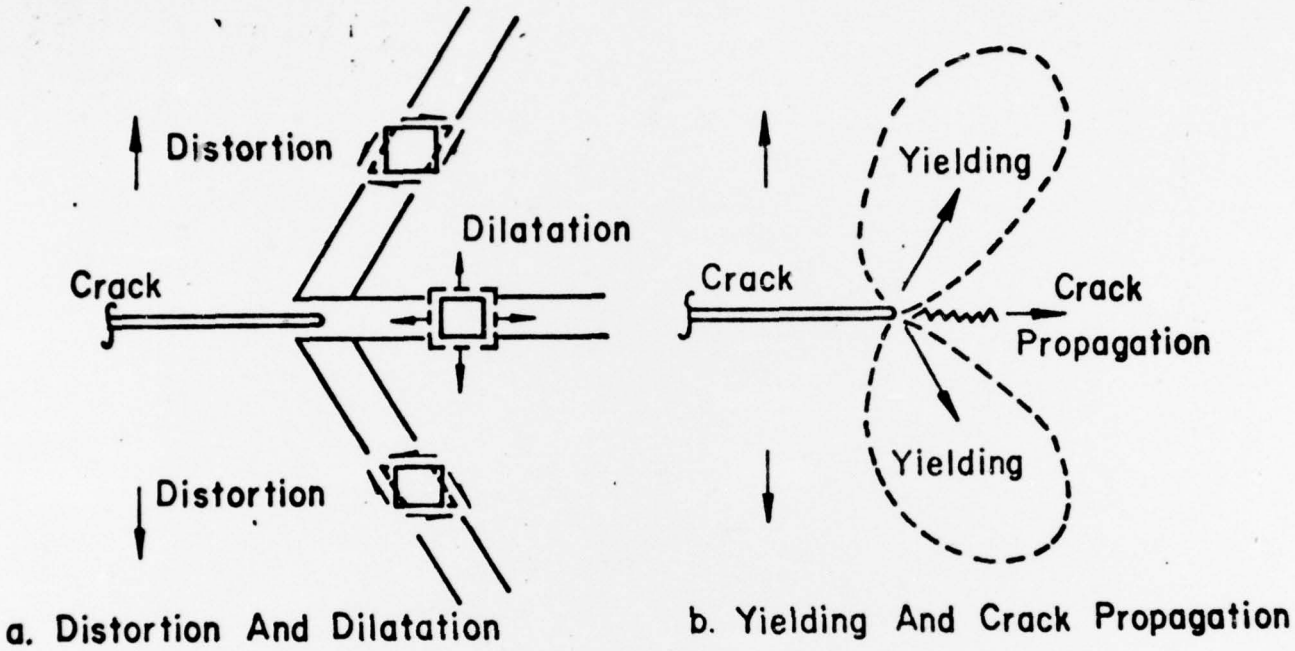

Fig. (4) - Zones of distortion and dilatation ahead of crack

Figures 5 show a central crack penetrating through eighty percent of the specimen width (a/b = 0.8) while its side has necked in about five percent of the crack length. The different degrees and pattern of yield are illustrated by the sequence of line drawings in Figures 5(a) to 5(f) in which σ_o/σ_{ys} is varied from 0.20 to 0.42. Yielding is assumed to take place when the effective stress σ_{eff} in a material element exceeds the yield stress σ_{ys}, i.e., $\sigma_{eff} > \sigma_{ys}$. The squares, triangles, etc., are used to signify the various intensities of yielding and the ranges within which they cover are defined as

$$\begin{aligned}
&\text{Square:} && \sigma_{ys} \leq \sigma_{eff} < \tfrac{1}{4}(\sigma_{max}-\sigma_{ys}) \\
&\text{Triangle:} && \tfrac{1}{4}(\sigma_{max}-\sigma_{ys}) \leq \sigma_{eff} < \tfrac{1}{2}(\sigma_{max}-\sigma_{ys}) \\
&\text{Plus symbol:} && \tfrac{1}{2}(\sigma_{max}-\sigma_{ys}) \leq \sigma_{eff} < \tfrac{3}{2}(\sigma_{max}-\sigma_{ys}) \\
&\text{Multiplication symbol:} && \tfrac{3}{2}(\sigma_{max}-\sigma_{ys}) \leq \sigma_{eff} \leq \sigma_{max}
\end{aligned} \qquad (5)$$

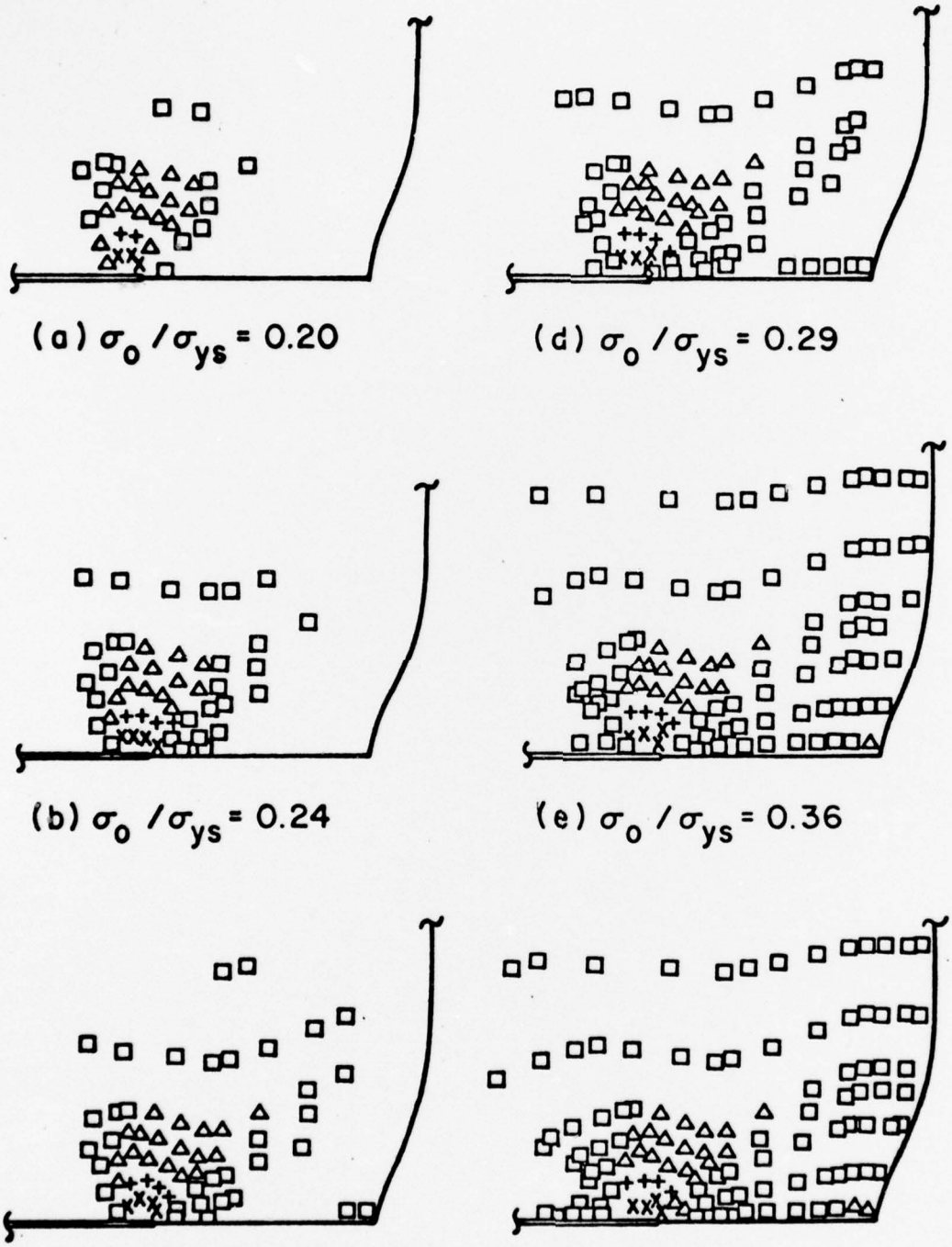

Fig. (5) - Yielding pattern of a 4 in x 4 in cracked specimen with a/b = 0.8 and σ_0/σ_{ys} varied from 0.20 to 0.42

Note that the plus and multiplication symbols represent intensified yielding and they occur in a region confined close to the crack tip. The intensity of yielding decreases with distances away from the crack tip until no yielding occurs. For σ_o/σ_{ys} = 0.20 and 0.24, the specimen is still elastic at large except for a localized zone. As the applied load is increased, the region next to the necked boundary begins to deform plastically leaving a path of elastic material at an angle. This is shown in Figures 5(c) and 5(d) where σ_o/σ_{ys} = 0.27 and 0.29. Further increase in σ_o leads to yielding of the entire section as indicated in Figures 5(e) and 5(f) for σ_o/σ_{ys} = 0.36 and 0.42. It is important to note that yielding is not uniform. The higher intensities occur near the crack tip and the necked boundary.

LAST LIGAMENT FAILURE

The pertinent question is whether the crack would run through the region of maximum plastic deformation (i.e., highest intensity of yielding) toward the specimen boundary or would attempt to avoid the deformed material, growing into the elastic zone in front of the tip and then diverging from the line of symmetry to break through the last ligament at an angle*. The strain energy density criterion [7] has been applied to predict the phenomenon of mixed mode fracture. The path of minimum strain energy density consistently lies between the region of maximum plastic yielding and the horizontal axis that connects the crack tip to the free surface for several specimen configurations. Figure 6 gives the result for a typical calculation where σ_o/σ_{ys} = 0.28 and a/b = 0.60. The theory predicts crack propagation along a path next to the inner elastic-plastic boundary intersecting the surface at an oblique angle.

Although the foregoing results must be regarded as preliminary, they are nevertheless helpful in gaining insights into the ductile fracture behavior of metals. An interpretation of fracture modes associated with the relative degrees of material ductility is given in Figures 7(a) to 7(d). The fracture path for a relatively brittle material is mostly flat with yielding localized to the crack tip region, Figure 7(a). In such a case, energy is dissipated predominantly due to the creation of a free or crack surface. The more ductile behavior will exhibit appreciable deformation through necking as in Figure 7(b). The path of fracture will tend to curve as the specimen boundary is approached. Since both Figures 7(a) and 7(b) show that crack extension prevails in the elastic portion of the material, the energy required to extend a unit crack extension at global instability must then be the same. This means that the same fracture toughness value must apply to the same material that exhibits either brittle or ductile behavior owing to changes in specimen size. In other words, material constants should not be sensitive to changes in geometry and size of specimens. A more detailed discussion on this topic can be found in [8,9]. For the very ductile

*In a cylindrical tensile bar, this last ligament forms the cup-and-cone as shown in Figure 1(c).

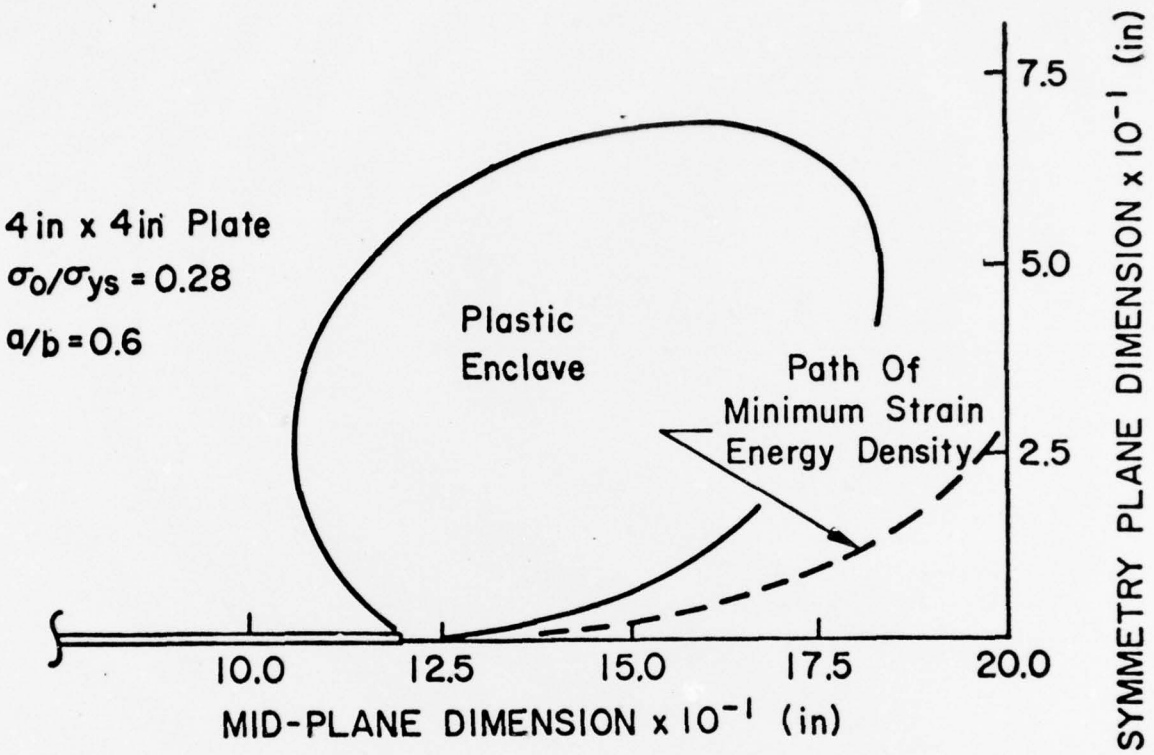

Fig. (6) - Last ligament failure predicted by the strain energy density criterion

materials* that undergo extensive deformation, it is possible to achieve net section yield, Figure 7(c). In that case, the fracture pattern will again be developed in accordance with the distribution of distortion and dilatation which can be predicted from the strain energy density theory. This is being referred to as the second degree of yielding in Figure 7(d). Refer to Figure 5(f) for the details of an actual elastic-plastic stress calculation. The specimen will of course be necked considerably by this time and the cup-and-cone when developed will be much smaller in size than that of the material in Figure 7(b). Continuum mechanics analysis is limited to sorting out the regions of distortion (yielding) from those of dilatation (crack growth as assumed in the strain energy density

*Ductility is known to increase with decreasing specimen size.

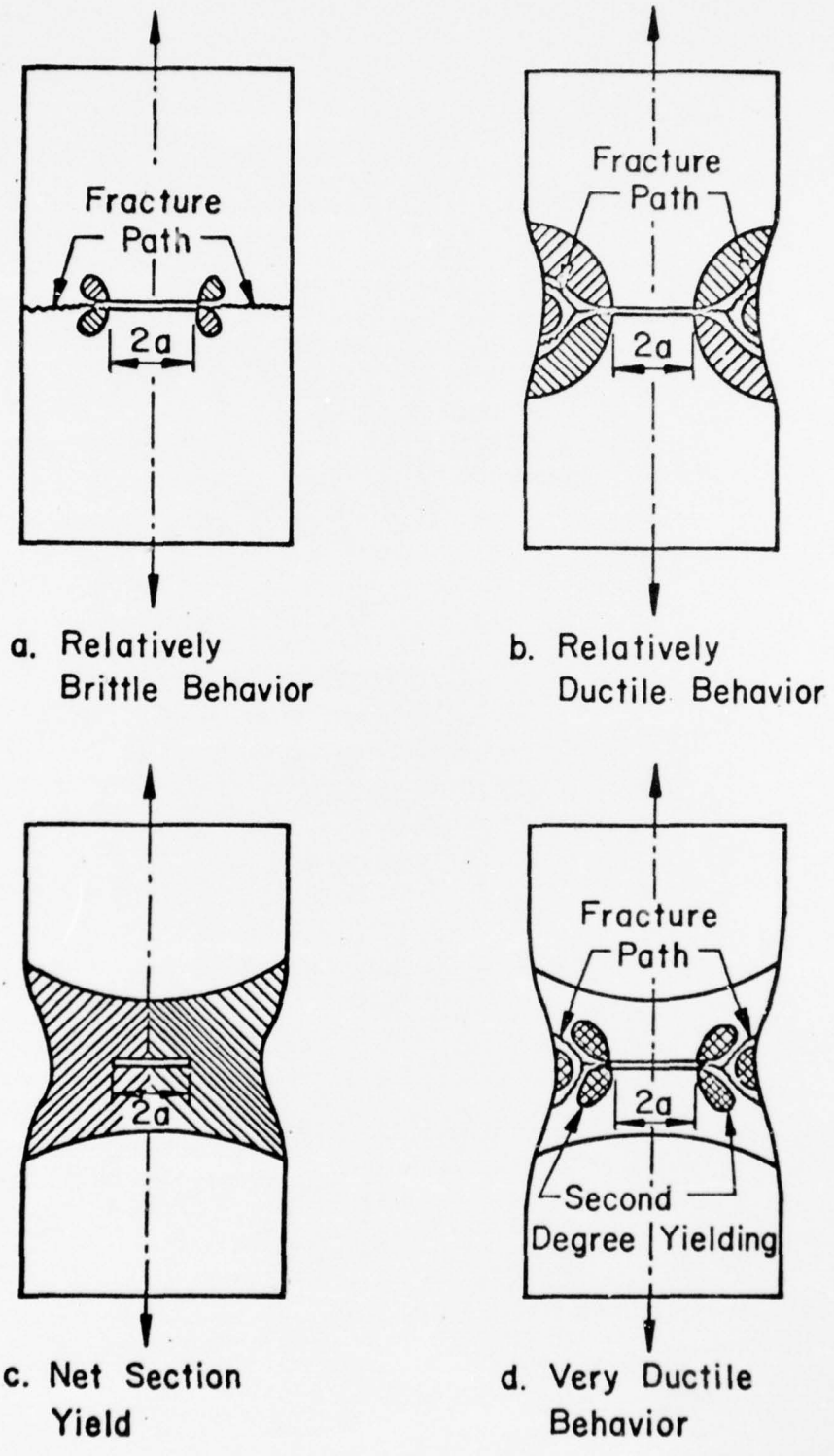

Fig. (7) - Brittle and ductile fracture modes

theory [7]). It is the proportion of energy dissipated through plastic deformation (micro surface creation) and fracture (macro free-surface creation) that determines the final fracture mode. Generally speaking, it is desirable to balance these two energy dissipations and hence structural members are often called to operate in the transition region, Figure (2) for plate specimens and Figure 7(b) for bar specimens.

An extensive amount of experimental work has been done [10] in the past to show that the critical strain energy density $(dW/dV)_c$ is characteristic of the material undergoing both elastic and plastic deformation. Once $(dW/dV)_c$ is known, analysis may be carried out to predict the allowable load and net section size of structural members that deform elastically and/or plastically. The relation $(dW/dV)_c = S_c/r_o$ can also be used to locate the distance r_o from the crack front at which failure initiates. The quantity S_c has been known as the critical strain energy density factor [7].

THREE DIMENSIONAL CRACK GROWTH PREDICTIONS

A three-dimensional finite element program for a through crack in a finite thickness plate has been developed [11] to examine the phenomenon of crack tunneling. The crack front may either be straight or curved depending on the constraint* of the plate surfaces. Calculations have been made for various crack front shapes in conjunction with crack growth modeling based on the strain energy density criterion. The stress distribution near the crack front is found to be sensitive to the details of the specimen geometry, material properties and loading. This suggests that the crack may adapt itself into a natural shape at which unstable fracture can occur**. Information on the size and shape of this crack at instability is pertinent to resolving the little understood problem of thickness size effect.

The aim of this work is to model the stable growth process in a ductile material by separately analyzing the influences of crack front geometry and the contributions from material nonlinearity. The influence of crack front curvature is first examined with the aid of a three-dimensional elastic finite element

---

* In the more ductile material where shear lips are developed the crack profile can be curved and grow appreciably before instability.

** Experimental observations [13] in the fracture of moderately thick plates loaded monotonically show that stable crack growth is first initiated in the specimen interior thereby increasing the front curvature. Instability or rapid crack propagation is observed to occur at about the time when the shear lips (nonplanar crack front growth) are developed.

analysis* [12] in conjunction with a local growth criterion to predict increments of crack growth and corresponding changes in crack front shape. In general, both the direction and magnitude of local crack growth from the current crack front are expected to vary with position along that front. The strain energy density field surrounding the crack front is the basis for the development of the local crack growth criterion [8,14]. It is postulated that the path of growth from each point along the crack edge will follow the minimum strain energy density path emanating from that point. Further, growth at points along the current crack front will initiate when the strain energy density at a "core" distance r_o along the minimum path reaches a preset value $(dW/dV)_c$.

Hence, the continuous growth of the crack front is approximated by discrete increments of growth. The amount of growth at a point along the crack front in an increment is taken to be the distance along the minimum strain energy density path, $(dW/dV)_{min}$, to the point where $(dW/dV)_{min}$ reaches a preset value**, $(dW/dV)_c$, which depends on the material properties. Figure 8 gives a descriptive

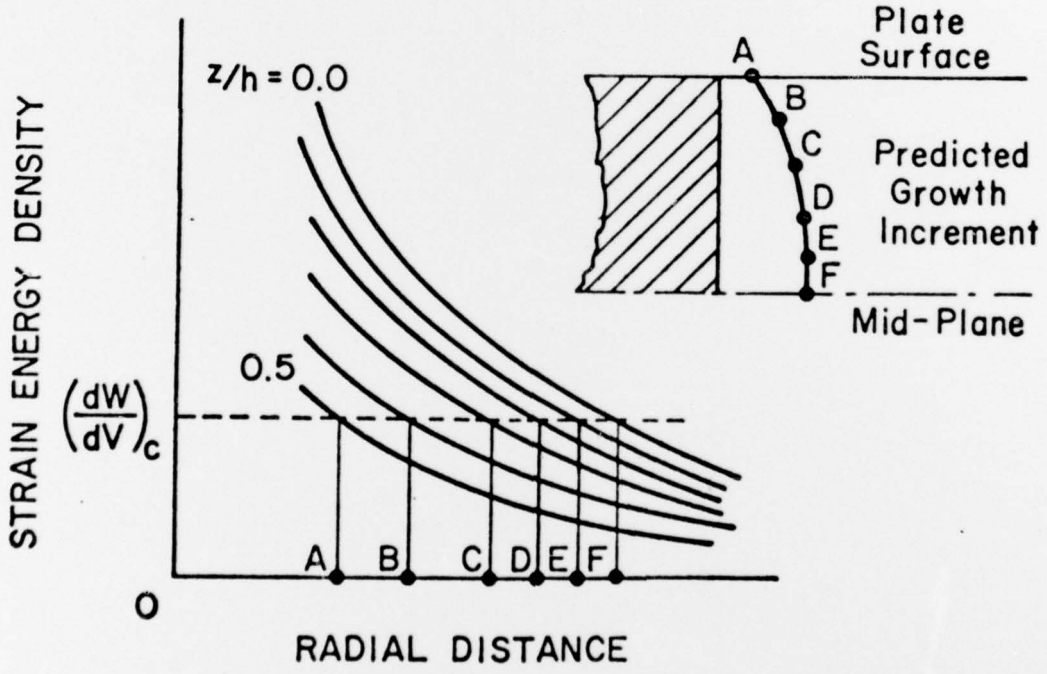

Fig. (8) - Crack growth prediction based on strain energy density

* The effect of material nonlinearity due to plasticity will be presented in another communication.

** This value of $(dW/dV)_c$ can be determined experimentally for a particular material [11].

plot of strain energy density $(dW/dV)_{min}$ against the radial distance r in a plane normal to the applied load from the associated points A, B,---, F on the crack front. The new crack profile is determined from the various values of r and z/h on the graph where $(dW/dV)_c$ intersects. The selected value of $(dW/dV)_c$ will obviously affect the magnitude of growth and shape of the subsequent crack fronts.

The numerical results for a specific example are shown in Figures 9 to 11.

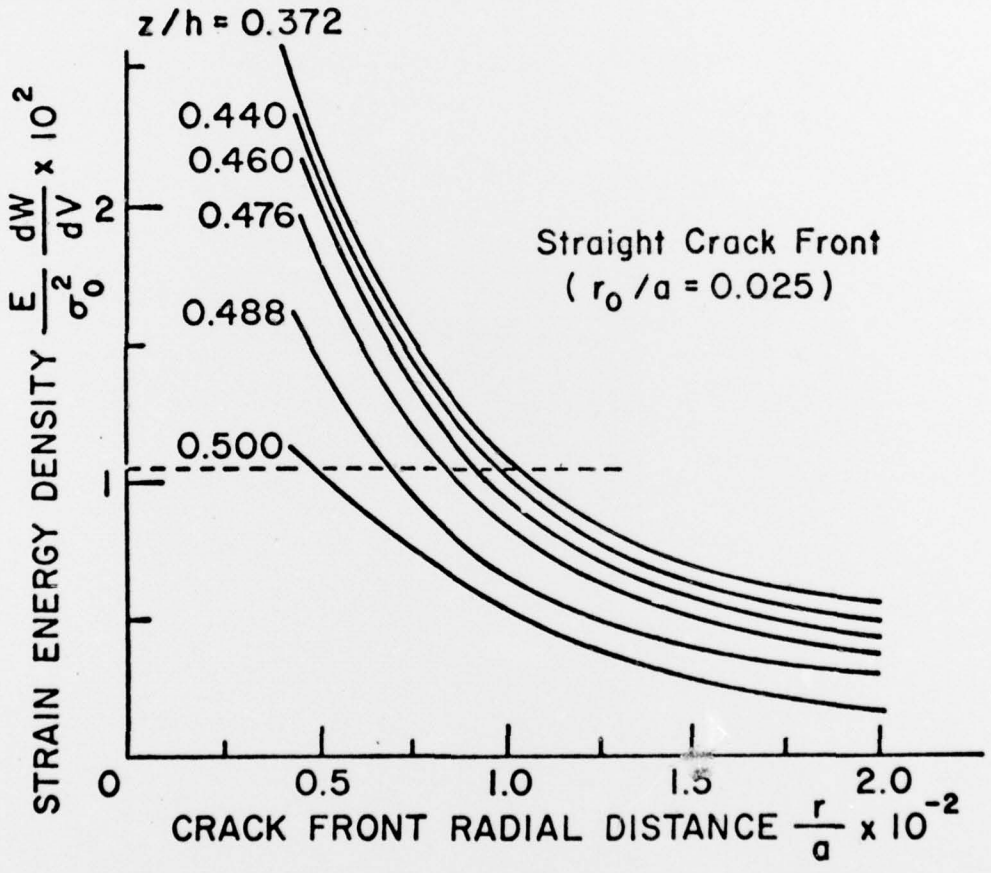

Fig. (9) - Strain energy density variation along a straight crack front

The normalized strain energy density $(E/\sigma_0^2)(dW/dV)$ is plotted as a function of r/a for different values of z/h where z is the thickness coordinate measured from the mid-plane. z/h = 0.5 locates the plate surface. Note that for a preset value of $(dW/dV)_c$ less changes in r are observed as z/h is decreased. This implies that the crack profile undergoes relatively small change in the specimen

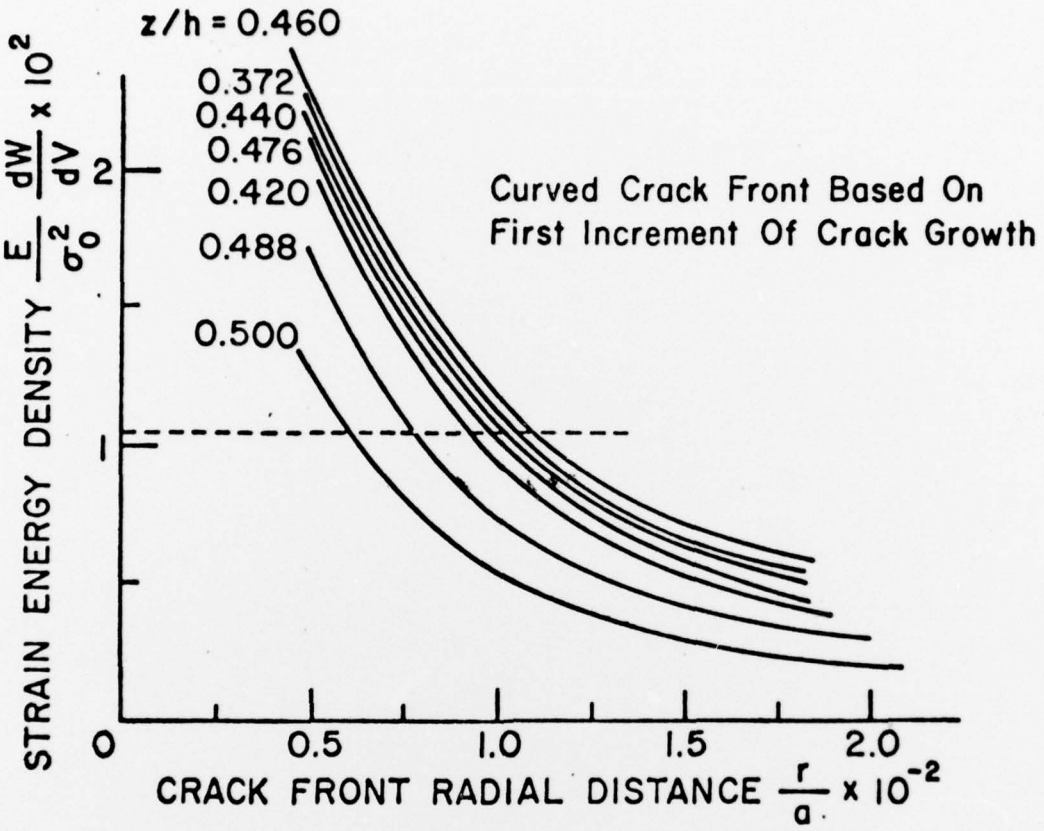

Fig. (10) - Strain energy density variation along a curved crack front - first increment of crack growth

interior while large changes are observed in regions close to the surface. Figure 12 displays the predicted crack front geometry with each increment of growth. The load level is kept constant during this period. The more pronounced crack curvature near the plate surface is indicative of the fact that the distortional component of strain energy density increases as the free surface is approached. This increase occurs even more rapidly for curved crack fronts than straight ones.

The results in Figures 9 to 12 explain in part why the material near the plate surface is more likely to yield and to cause the development of shear lips which in turn provide the constraint to contain crack growth. Crack tunneling is a consequence of this surface constraint, Figure 13(a). The point at which the crack overcomes this constraint corresponds to global instability, Figure 13(b), of the specimen; that is, when the specimen looses its structural integrity. It should be cautioned that nonlinear load-displacement response in the global sense may not always correspond to material nonlinearity. In this

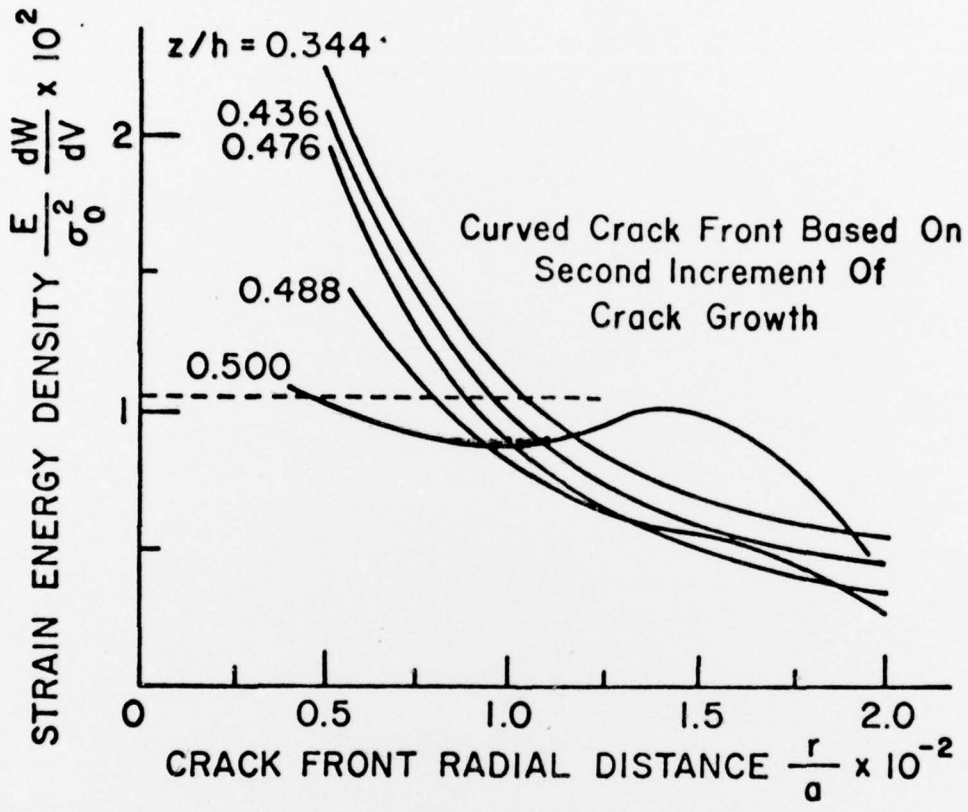

Fig. (11) - Strain energy density variation along a curved crack front - second increment of crack growth

case, the influence can be attributed to changes in crack geometry. As mentioned earlier, the contribution of material nonlinearity is currently under study.

At this point, a few remarks with regard to adding a crack-length increment (that is equal to the calculated one-dimensional plastic-zone size) onto the original crack length may be in order. This is the usual procedure in fracture mechanics to correct for plasticity effects. In view of the results of this investigation, it might be more appropriate to add an average half crack length a_c as in Figure 13(a) with $2(a+a_c)$ being the effective crack length. The correction a_c can be obtained simply by equating the shaded area inside and outside the tunnel crack. Once the phenomenon of ductile fracture is understood and the shape and size of these tunneling cracks are calculated for a variety of situations, there is no difficulty in establishing simple engineering formulas for design applications.

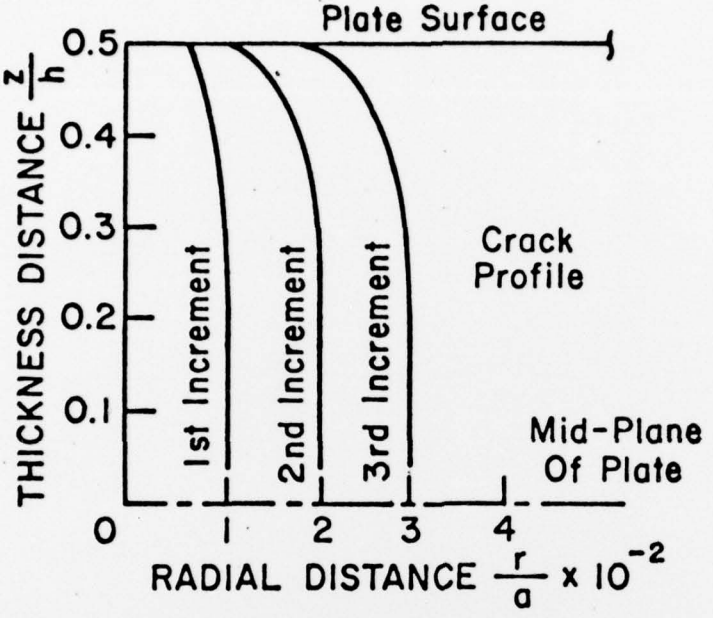

Fig. (12) - Predicted increments of crack growth

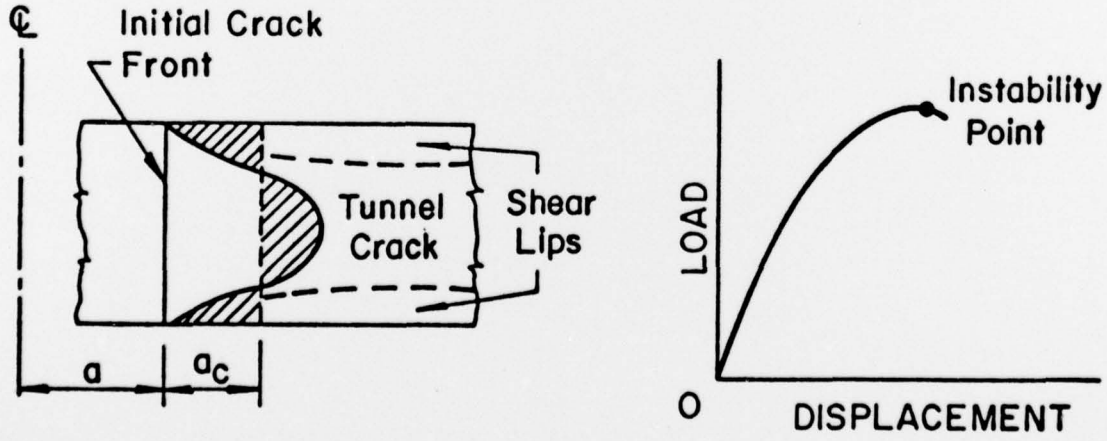

(a) Effective crack length at instability

(b) Non-linear response

Fig. (13) - Nonlinear effect due to crack tunneling

ACKNOWLEDGEMENT

The author gratefully acknowledges the financial support of the Office of Naval Research under Contract N00014-76-C-0094 which has made this study possible.

REFERENCES

[1] Sih, G. C. and Erdogan, F., "Stress intensity factor: concept and application", Linear Fracture Mechanics, edited by G. C. Sih, R. P. Wei and F. Erdogan, Envo Publishing Co., Inc., p. 85, 1975.

[2] Sih, G. C., "Effect of nonalignment of load on crack propagation", Transactions of the 3rd International Conference on Structural Mechanics in Reactor Technology, Vol. 5, p. L718, 1975.

[3] Sih, G. C., "Application of the strain energy density theory to fundamental fracture problems", Proceedings of the 10th Annual Meeting of the Society of Engineering Science, Raleigh, North Carolina, p. 221, 1973.

[4] Plane Strain Crack Toughness Testing of High Strength Metallic Materials, edited by W. F. Brown, Jr. and J. E. Srawley, ASTM Special Technical Publication, No. 410, 1966.

[5] Hilton, P. D., Sih, G. C. and Kiefer, B. V., "Growth characteristics of a through crack in a plate specimen", Technical Report IFSM-76-76, Lehigh University, June 1975.

[6] Hutchinson, J. W., "Plastic stress and strain fields at a crack tip", J. Mech. Physics and Solids, Vol. 16, p. 337, 1968.

[7] Sih, G. C., "A special theory of crack propagation", Methods of Analysis and Solutions of Crack Problems, Vol. 1, edited by G. C. Sih, Noordhoff International Publishing, Leyden, The Netherlands, p. 21, 1973.

[8] Sih, G. C., "Elastic-plastic fracture mechanics", Prospects of Fracture Mechanics, edited by G. C. Sih, H. C. van Elst and D. Broek, Noordhoff International Publishing, Leyden, The Netherlands, p. 613, 1974.

[9] Sih, G. C., "Fracture toughness concept", ASTM Special Technical Publication, No. 605, p. 3, 1976.

[10] Gillemot, L. F., "Criterion of crack initiation and spreading", J. of Engin. Fract. Mech., Vol. 8, p. 239, 1976.

[11] Sih, G. C., Hilton, P. D., Hartranft, R. J. and Kiefer, B. V., "Three-dimensional stress analysis of a finite slab containing a transverse central crack", Technical Report IFSM-75-69, Lehigh University, June 1975.

[12] Miller, G. A. and Stephenson, E. T., "The effect of the carbide phases on the crack growth of 0.5% Mo-B steels under impact, cyclic, and monotonically increasing loading", Metallurgical Transactions, Vol. 5, p. 659, 1974.

[13] Sih, G. C., "A three-dimensional strain energy density factor theory of crack propagation", Three-Dimensional Crack Problems, Vol. 2, edited by G. C. Sih, Noordhoff International Publishing, Leyden, The Netherlands, p. 15, 1975.

REPORT DOCUMENTATION PAGE		READ INSTRUCTIONS BEFORE COMPLETING FORM
1. REPORT NUMBER IFSM-77-78	2. GOVT ACCESSION NO.	3. RECIPIENT'S CATALOG NUMBER
4. TITLE (and Subtitle) Mechanics of Ductile Fracture		5. TYPE OF REPORT & PERIOD COVERED Technical Report 6. PERFORMING ORG. REPORT NUMBER
7. AUTHOR(s) G. C. Sih		8. CONTRACT OR GRANT NUMBER(s) N00014-76-C-0094
9. PERFORMING ORGANIZATION NAME AND ADDRESS Institute of Fracture and Solid Mechanics, Lehigh University Bethlehem, Pennsylvania 18015		10. PROGRAM ELEMENT, PROJECT, TASK AREA & WORK UNIT NUMBERS NR 064-562
11. CONTROLLING OFFICE NAME AND ADDRESS Department of the Navy Office of Naval Research Arlington, Virginia 22217		12. REPORT DATE June 1977 13. NUMBER OF PAGES 20
14. MONITORING AGENCY NAME & ADDRESS(if different from Controlling Office)		15. SECURITY CLASS. (of this report) Unclassified 15a. DECLASSIFICATION/DOWNGRADING SCHEDULE
16. DISTRIBUTION STATEMENT (of this Report) Approved for public release; distribution unlimited.		
17. DISTRIBUTION STATEMENT (of the abstract entered in Block 20, if different from Report)		
18. SUPPLEMENTARY NOTES		
19. KEY WORDS (Continue on reverse side if necessary and identify by block number) Crack tunneling Ductile fracture Crack growth Strain energy density		
20. ABSTRACT (Continue on reverse side if necessary and identify by block number) The phenomenon of ductile fracture in plate specimens is described by a finite element stress analysis coupled with the strain-energy density fracture criterion. The last ligament of failure tends to curve developing a cup-and-cone type of fracture in tensile bars and sheer lips in plate specimens. Three-dimensional crack growth profiles are developed by assuming that materials tend to break along the path of minimum strain energy density whose critical value is characteristic of the material and has been		

measured experimentally for both elastic and plastic materials. The results are encouraging in that ductile fracture behavior can be modeled by holding the strain energy density constant. Hence, allowable load and net section size can be predicted for specimens that deform in the plastic range.

DISTRIBUTION LIST

PART I - GOVERNMENT

Administrative and Liaison Activities

Chief of Naval Research
Department of the Navy
Arlington, Virginia 22217
Attn: Code 439 (3)
461
444

Director
ONR Branch Office
495 Summer Street
Boston, Massachusetts 02210

Director
ONR Branch Office
536 South Clark Street
Chicago, Illinois 60605

Director
Naval Research Laboratory
Attn: Library, Code 2029 (ONRL)
Washington, D.C. 20390 (6)

U.S. Naval Research Laboratory
Attn: Technical Information Division
Washington, D.C. 20390 (6)

Commanding Officer
ONR Branch Office
207 West 24th Street
New York, New York 10011

Director
ONR Branch Office
1030 E. Green Street
Pasadena, California 91101

Defense Documentation Center
Cameron Station
Alexandria, Virginia 22314 (12)

Navy

Chief of Naval Operations
Department of the Navy
Washington, D.C. 20305
Attn: NOP-05F
NOP-506N
NOP-098T

Headquarters
U.S. Marine Corps
Washington, D.C. 20380
Attn: MC-AX-2 (2)
MC-AX-4E2
MC-AAP-3

Commander
Naval Air Systems Command
Department of the Navy
Washington, D.C. 20360
Attn: NAVAIR-320N
NAVAIR-5302
NAVAIR-531
NAVAIR-5311J
NAVAIR-5314
NAVAIR-5325A

Commander
Naval Air Development Center
Warminster, Pennsylvania 18974
Attn: Mr. M. Schulman
Crew Systems Department

Naval Air Development Center
Philadelphia, Pennsylvania 19112
Attn: Dr. E. Hendler
Crew Systems Department

Director
Naval Research Laboratory
Washington, D.C. 20390
Attn: Code 8440 (Dr. F. Rosenthal)

Commanding Officer
Naval Ship Research and Development Center
Bethesda, Maryland 20034
Attn: Code 745 (Mr. B. Whang)

Commanding Officer
Naval Civil Engineering Laboratory
Port Hueneme, California 93041
Attn: Dr. Warren Shaw, Structures Department

Commander
Naval Safety Center
Naval Air Station
Norfolk, Virginia 23511

Capt. Channing L. Ewing Mclusn
Naval Aerospace Medical Research Laboratory
Michoud Assembly Facility
New Orleans, Louisiana 70129

Army

Commanding Officer
U.S. Army Aviation Material Laboratories
Fort Eustis, Virginia 23604
Attn: VDLEU-SS
(Mr. G. T. Singley, III)

Director
U.S. Army Board for Aviation Accident Research
Fort Rucker, Alabama 36360
Attn: BAAR-PP (Mr. J. Haley)

Commanding Officer
U.S. Army Research Office Durham
Attn: Mr. J. J. Murray
CRD-AA-IP
Box CM, Duke Station
Durham, North Carolina 27706

Air Force

Air Force Office of Scientific Research
1400 Wilson Boulevard
Arlington, Virginia 22209
Attn: Mechs. Div.

Commanding Officer
6571st AMRL
Holloman Air Force Base, New Mexico
Attn: Mr. C. C. Gragg

NASA

Mr. C. Kubokawa
N239-3
NASA Ames Research Center
Moffett Field, California 94035

Department of Transportation

Mr. R. F. Chandler
Code AC 119
CAMI, FAA Aeronautical Center
P.O. Box 25082
Oklahoma City, Oklahoma 73123

Mr. H. Spicer
Federal Aviation Administration (DS-41)
800 Independence Avenue, S.W.
Washington, D.C. 20590

Mr. H. Daiutolo
Federal Aviation Administration
NAFEC (NA541)
Atlantic City, New Jersey 08405

Mr. D. Beyer
Federal Aviation Administration (RD-730)
800 Independence Avenue, S.W.
Washington, D.C. 20590

Headquarters
U.S. Coast Guard
400 7th Street, S.W.
Washington, D.C. 20590
Attn: DAT/62
EAE/63
ENE-5/64
IGS-1/61
NMT-t/82
OSR-2/73

Mr. J. G. Viner
Protective Systems Group (RS-12)
Federal Highway Administration
400 7th Street, S.W.
Washington, D.C. 20590

Mr. W. H. Collins
Computer Technology Group (DV-11)
Federal Highway Administration
400 7th Street, S.W.
Washington, D.C. 20590

Mr. Kenneth Batcheller, Chief
Safety Programs Division (RS-20)
Federal Railroad Administration
400 7th Street, S.W.
Washington, D.C. 20590

Mr. E. Ward, Chief
Engineering Research and Development
Division (RT-20)
Federal Railroad Administration
400 7th Street, S.W.
Washington, D.C. 20590

Dr. J. A. Edwards
Associate Administrator for Research
and Development
National Highway Traffic Safety
Administration
400 7th Street, S.W.
Washington, D.C. 20590

Mr. C. D. Ferguson
Office of Crashworthiness (41-40)
National Highway Traffic Safety
Administration
400 7th Street, S.W.
Washington, D.C. 20590

Mr. L. L. Bradford
Office of Vehicle Structures Research
(43-50)
National Highway Traffic Safety
Administration
400 7th Street, S.W.
Washington, D.C. 20590

National Transportation Safety Board
800 Independence Avenue, S.W.
Washington, D.C. 20590
Attn: Mr. A. L. Schmieg, NS-10
Mr. H. L. Morgan, NS-20
Mr. B. C. Doyle, NA-87

Dr. H. E. vonGierke
Aerospace Medical Research
Laboratory
Aerospace Medical Division
Air Force Systems Command
Wright-Patterson Air Force Base,
Ohio 45433

Part II - CONTRACTORS AND OTHER
TECHNICAL COLLABORATORS

Mr. S. P. Desjardins
Dynamic Science
1800 West Deer Valley Drive
Phoenix, Arizona 85027

Dr. A. A. Ezra, Chairman
Department of Mechanical Sciences
and Environmental Engineering
University of Denver
Denver, Colorado 80210

Dr. Albert I. King
Bioengineering Center
Wayne State University
Detroit, Michigan 48202

Dr. R. C. DeHart, Director
Department of Structural Research
Southwest Research Institute
P.O. Drawer 28510
San Antonio, Texas 78284

Professor J. B. Martin
Division of Engineering
Brown University
Providence, Rhode Island 02912

Dr. J. L. Tocher
Boeing Computer Services (72-80)
P.O. Box 24346
Seattle, Washington 98124

Mr. D. G. Harding, Manager
Survivability Staff
Boeing Company - Vertol Division
Philadelphia, Pennsylvania 19142

Dr. H. E. Lindberg, Manager
Engineering Mechanics Program
Stanford Research Institute
Menlo Park, California 94025

Mr. John W. Freyler
Beta Industries, Inc.
2763 Culver Avenue
Dayton, Ohio 45429

Dr. L. E. Hulbert, Chief
Advanced Solid Mechanics Division
505 King Avenue
Columbus, Ohio 43201

Professor George Sih
Department of Mechanics
Lehigh University
Bethlehem, Pennsylvania 18015

Dr. Harold Liebowitz, Dean
School of Engineering and
Applied Science
George Washington University
725 23rd Street
Washington, D.C. 20006

Professor S. B. Dong
University of California
Department of Mechanics
Los Angeles, California 90024

Professor A. J. Durelli
Mechanics Division
The Catholic University of
America
Washington, D.C. 20017

Professor H. H. Bleich
Department of Civil Engineering
Columbia University
Amsterdam & 120th Street
New York, New York 10027

Professor A. M. Freudenthal
George Washington University
School of Engineering and
Applied Science
Washington, D.C. 20006

Professor P. G. Hodge
Department of Mechanics
University of Minnesota
Minneapolis, Minnesota 55455

Professor D. C. Drucker
Dean of Engineering
University of Illinois
Urbana, Illinois 61801

Professor N. M. Newmark
Department of Civil Engineering
University of Illinois
Urbana, Illinois 61801

Library (Code 0384)
U.S. Naval Postgraduate School
Monterey, California 93940

Dr. Francis Cozzarelli
Division of Interdisciplinary Studies
and Research
School of Engineering
State University of New York
Buffalo, New York 14214

Dr. George Herrmann
Stanford University
Department of Applied Mechanics
Stanford, California 94305

Professor J. D. Achenbach
Technological Institute
Northwestern University
Evanston, Illinois 60201

Professor J. Kempner
Department of Aero. Engrg. and
Applied Mech.
Polytechnic Institute of Brooklyn
333 Jay Street
Brooklyn, New York 11201

Dr. Nicholas J. Hoff
Dept. of Aero. and Astro.
Stanford University
Stanford, California 94305

Professor Norman Jones
Massachusetts Institute of Tech-
nology
Department of Naval Architecture
and Marine Engineering
Cambridge, Massachusetts 02139

Professor Werner Goldsmith
Department of Mechanical
Engineering
Division of Applied Mechanics
University of California
Berkeley, California 94720

Professor W. D. Pilkey
Department of Aerospace Engineering
University of Virginia
Charlottesville, Virginia 22903

Dr. H. N. Abramson
Southwest Research Institute
8500 Culebra Road
San Antonio, Texas 78206

Mr. John Scowcroft
Automobile Manufactures Association
330 New Center Building
Detroit, Michigan 48202

Dr. R. D. Young
Texas Transportation Institute
Texas A & M University
College Station, Texas 77840

Professor J. A. Collins
Mechanical Engineering Department
Arizona State University
Tempe, Arizona 85281